Journal of Alloys and Compounds 501 (2010) 245–254

Contents lists available at ScienceDirect

Journal of Alloys and Compounds

journal homepage: www.elsevier.com/locate/jallcom

Studies of $Ti_{1.5}Zr_{5.5}V_{0.5}(M_xNi_{1-x})_{9.5}$ (M = Cr, Mn, Fe, Co, Cu, Al): Part 2. Hydrogen storage and electrochemical properties

K. Young[a,*], J. Nei[b], B. Huang[a], T. Ouchi[a], M.A. Fetcenko[a]

[a] Energy Conversion Devices Inc./Ovonic Battery Company, 2983 Waterview Drive, Rochester Hills, MI 48309, USA
[b] Department of Chemical Engineering, Wayne State University, Detroit, MI 48202, USA

ARTICLE INFO

Article history:
Received 12 March 2010
Received in revised form 1 April 2010
Accepted 8 April 2010
Available online 24 April 2010

Keywords:
Hydrogen absorbing materials
Transition metal alloys
Metal hydride electrode
Electrochemical reactions

ABSTRACT

In Part 2 of this two part series of papers, the gas phase and electrochemical properties of the quinary alloy $Ti_{1.5}Zr_{5.5}V_{0.5}(M_xNi_{1-x})_{9.5}$ with M = Cr, Mn, Fe, Co, Cu, or Al and $x = 0.1$ or 0.2 are studied and compared to the structural properties reported in Part 1. The electrochemical properties of the alloys are strongly related to the non-Laves phases. For example, the Zr_7Ni_{10} phase provides a more catalytic surface and improves the high rate discharge capability of the alloy at the expense of discharge capacity due to the higher Ni to Zr ratio; the Zr_9Ni_{11} phase, on the contrary, improves the discharge capacity but hinders the high rate discharge capability. In the Laves phases, C14 provides a stable hydride with lower equilibrium pressure, higher gas phase storage capacity and lower electrochemical rate capability. The C15 phase provides a less stable hydride with higher equilibrium pressure, lower gas phase storage capacity and higher electrochemical storage capacity. The main effect of each modifying element can be summarized as follows: Mn is the most beneficial substitution element found in this study. Mn increases both the gas phase and electrochemical capacities with good reversibility; it also improves the activation, hydrogen diffusion, surface reaction, and high rate discharge capability. Co increases the degree of disorder in the alloy, reduces both gas phase and electrochemical capacities, destabilizes the hydride, improves activation, and reduces surface reactivity. Fe decreases the gas phase capacity but improves the electrochemical discharge capacity. Fe facilities activation, but its surface reaction is the least active among the substituents used in this study. Al, Cr, and Cu are less desirable because they reduce: (1) the electrochemical and gas phase capacities, (2) the reversibility, and (3) the rate capability. They also slow activation.

1. Introduction

Both gas phase and electrochemical hydrogen storage capabilities of Zr_7Ni_{10} based alloys are promising [1–3], leading to a series of studies investigating the potential use of Zr_7Ni_{10} based alloys as the metal hydride electrode active material in nickel metal hydride batteries [4–6]. Due to their abundant number of constituent phases (Zr_7Ni_{10}, Zr_9Ni_{11}, C14, C15, ZrNi, $ZrNi_3$, ZrO_2, etc.), Zr_7Ni_{10} based alloys are good candidates for studying the synergetic effects among adjacent storage phases and catalytic phases. In Part 1 of this paper, the microstructures of a series of quinary alloys $Ti_{1.5}Zr_{5.5}V_{0.5}(M_xNi_{1-x})_{9.5}$ with M = Cr, Mn, Fe, Co, Cu, or Al and $x = 0.1$ or 0.2 were reported [6]. All 12 alloy samples are multiphase and composed of at least one Laves phase (C14 or C15) and at least one Zr–Ni non-Laves phase. Only partial substitution with Cu maintains the Zr_7Ni_{10}-dominant microstructure. Substitution of elements with fewer outer shell electrons, such as Al, Mn, and Cr were found to promote more C14 phase, while Fe and Co favored the C15 structure. The average electron density (e/a value) was found to play a determining role in the preferential formation of the C14 or C15 phase. As the Ni-content of the alloy decreases, the structure of the non-Laves phase changes from Zr_7Ni_{10} to $Zr_7Ni_{10} + Zr_9Ni_{11}$, then to Zr_9Ni_{11}, and finally to $Zr_9Ni_{11} + ZrNi$. The solubilities of V and Cr in the Zr_7Ni_{10} and Zr_9Ni_{11} phases are very low, and the contents of the other substituting elements in these phases are also lower than those found in Laves phases.

Continuing from Part 1, this paper presents both the gas phase and electrochemical storages of the same series of quinary alloys. These properties are compared and correlated to the structural characteristics reported in Part 1. The impacts of each constituent phase and modifier element to the storage properties will be discussed.

2. Experimental setup

Samples were made by arc melting under a continuous argon flow with a non-consumable tungsten electrode and a water-cooled

* Corresponding author. Tel.: +1 248 293 7000; fax: +1 248 299 4520.
E-mail address: kwoyoung@yahoo.com (K. Young).

0925-8388/$ – see front matter © 2010 Elsevier B.V. All rights reserved.
doi:10.1016/j.jallcom.2010.04.078

Table 1
Summary of gas phase and electrochemical properties of alloys in this study. The calculations of entropy and enthalpy for alloys Al1 and Al2 do not yield satisfactory results due to errors in determining the plateau pressure.

Alloy number	Alloy formula	Max H-storage at 60 °C	Reversible H-storage at 60 °C	Mid-point pressure at 60 °C des. (MPa)	60 °C PCT slope factor	$\beta \rightarrow \gamma$ ΔH in kJ/mol	$\beta \rightarrow \gamma$ ΔS in J/K mol	Total capacity (mAh/g)	High rate dischargeability at cycle 10	Diffusion coefficient, D ($\times 10^{-10}$ cm^2/s)	Exchange current I_0 (mA/g)
ZN07	$Ti_{1.5}Zr_{5.5}V_{0.5}Ni_{9.5}$	1.32%	0.69%	0.076	0.53	−26	−83	242	80%	18.9	24.7
Cr1	$Ti_{1.5}Zr_{5.5}V_{0.5}Cr_{0.95}Ni_{8.55}$	1.30%	0.57%	0.042	0.33	−25	−72	203	44%	10.1	6.3
Cr2	$Ti_{1.5}Zr_{5.5}V_{0.5}Cr_{1.9}Ni_{7.6}$	1.72%	0.44%	0.10	0.56	−38	−114	194	51%	19.4	8.5
Mn1	$Ti_{1.5}Zr_{5.5}V_{0.5}Mn_{0.95}Ni_{8.55}$	1.35%	0.73%	0.079	0.59	−28	−81	274	71%	21.5	8.9
Mn2	$Ti_{1.5}Zr_{5.5}V_{0.5}Mn_{1.9}Ni_{7.6}$	1.60%	1.01%	0.038	0.75	−42	−118	349	85%	42.4	14.4
Fe1	$Ti_{1.5}Zr_{5.5}V_{0.5}Fe_{0.95}Ni_{8.55}$	1.11%	0.63%	0.13	0.48	−25	−79	246	44%	7.9	5.4
Fe2	$Ti_{1.5}Zr_{5.5}V_{0.5}Fe_{1.9}Ni_{7.6}$	1.12%	0.65%	0.14	0.49	−24	−76	293	71%	8.1	6.7
Co1	$Ti_{1.5}Zr_{5.5}V_{0.5}Co_{0.95}Ni_{8.55}$	1.18%	0.68%	0.13	0.47	−23	−72	212	78%	14.8	5.5
Co2	$Ti_{1.5}Zr_{5.5}V_{0.5}Co_{1.9}Ni_{7.6}$	1.00%	0.59%	0.12	0.46	−17	−54	178	77%	22.7	9.2
Cu1	$Ti_{1.5}Zr_{5.5}V_{0.5}Cu_{0.95}Ni_{8.55}$	1.35%	0.77%	0.088	0.54	−29	−87	87	100%	10.4	9.1
Cu2	$Ti_{1.5}Zr_{5.5}V_{0.5}Cu_{1.9}Ni_{7.6}$	1.26%	0.56%	0.15	0.39	−64	−126	175	73%	14.8	8.5
Al1	$Ti_{1.5}Zr_{5.5}V_{0.5}Al_{0.95}Ni_{8.55}$	1.17%	0.48%	0.078	0.53	N.A.	N.A.	252	50%	19.1	11.8
Al2	$Ti_{1.5}Zr_{5.5}V_{0.5}Al_{1.9}Ni_{7.6}$	1.05%	0.50%	0.025	0.38	N.A.	N.A.	160	29%	9.1	11.1

copper tray. Before each arc melt, a piece of sacrificial titanium underwent a few melting–cooling cycles to reduce the residual oxygen concentration in the system. Each 10-g sample ingot was re-melted and flipped over a few times to ensure uniformity in chemical composition. Pressure–Concentration–Temperature (PCT) characteristics for each sample were measured using a Suzuki-Shokan multi-channel PCT system. In the PCT analysis, each sample was first activated by a 2-h thermal cycle between 300 °C and room temperature in 25 atm. of hydrogen.

To prepare for the discharge capacity and electrochemical studies, each ingot sample was ground and sized using a 200-mesh sieve. The sieved powder was then compacted onto an expanded nickel substrate by a 10-ton press to form a test electrode (about 1 cm^2 in area and 0.2 mm thick) without binder. Electrochemical measurements were performed with a Solartron 1470 cell test multi-channel potentiostat and a Solartron 1250 Frequency Response Analyzer. Discharge capacity of each small sized electrode was measured in a flooded cell configuration using a partially pre-charged $Ni(OH)_2$ sintered electrode as the positive electrode and a 6 M KOH solution as the electrolyte. The system was charged at a current density of 50 mA/g for 6 h and then discharged at a current density of 50 mA/g until a cut-off voltage of −0.9 V was reached. The system was then discharged at a current density of 12 mA/g until a cut-off voltage of −0.9 V was reached and finally discharged at a current density of 4 mA/g until a cut-off voltage of −0.9 V was reached. Linear polarization was performed by scanning the potential from −20 mV to +20 mV of the open circuit voltage at a rate of 0.1 mV/s. For the potentiostatic discharge experiments, electrodes in a fully charged state were polarized +0.6 V vs. open circuit voltage for 5400 s.

3. Results and discussion

The hydrogen storage properties of alloys can be studied by observing both the gas phase reaction with hydrogen and the electrochemical reaction in a chemical environment. The PCT isotherm obtained from the gas phase reaction can be related to the open circuit voltage plotted against the state of charge by the Nernst equation [7,8]:

$$V\,(\text{vs. Hg/HgO}) = -0.932 - 0.0296\,(\log p(H_2)) \quad (1)$$

There are at least two major differences between the gas phase and the electrochemical environment. In the gas phase, hydrogen transport is mainly driven by the concentration against the metal surface acting as catalysis [9,10]. In electrochemical testing, both concentration gradient and applied voltage govern hydrogen transport with catalysis from the metallic inclusions imbedded in the surface oxide [10–14]. Storage capacity during electrochemical discharge may be converted to hydrogen storage capacity and is

Table 2
Correlation coefficients between the measured properties and the phase abundances from XRD analysis. A positive (negative) correlation coefficient indicates a positive (negative) correlations. Numbers in **bold** are significant with a correlation coefficient greater than 0.3.

	Zr_7Ni_{10}	Zr_9Ni_{11}	C14	C15	ZrNi
Max. H-storage	−0.04	0.06	**0.30**	**−0.44**	**0.65**
Reversible H-storage	0.07	−0.10	−0.11	0.18	**−0.40**
Mid-point pressure	0.30	−0.28	**−0.71**	**0.45**	0.06
ΔH	0.06	0.15	**−0.78**	**0.54**	0.02
ΔS	0.04	0.17	**−0.76**	**0.54**	0.02
PCT slope factor	−0.09	−0.06	0.18	−0.01	0.17
Max. dis. capacity	**−0.45**	**0.36**	0.07	**0.40**	−0.12
HRD	**0.51**	**−0.40**	**−0.48**	0.05	−0.22
Diffusion coefficient	−0.17	0.10	**0.31**	−0.13	0.08
Exchange current	**0.40**	**−0.45**	0.15	**−0.40**	−0.09

usually between the reversible gas phase storage (within a practical pressure range, typically 0.1 to a few atm) and the maximum gas phase storage capacity (i.e. reversible and non-reversible). In general, results from both measurements are highly correlated [15]. However, an exception due to changes in surface catalytic activities has been previously reported [16]. Table 1 summarizes all of the gas phase and electrochemical properties measured of the tested alloys. Table 2 shows the correlation coefficients (CC) linking these properties to the phase abundances reported in Part 1 of this series of papers [6]. A positive CC indicates a positive correlation. A larger CC corresponds to a stronger correlation. The significant CCs (those with an absolute value greater than 0.3) are highlighted in bold in Table 2.

3.1. Hydrogen gas storage properties

Gas phase hydrogen storage properties of the alloys were studied by PCT. The resulting absorption and desorption isotherms measured at 60 and 90 °C are shown in Figs. 1 and 2, respectively. The PCT isotherm of the base alloy (ZN07) is also included in each graph for ease of comparison. Due to slow kinetics at 30 °C, equilibrium was difficult to reach under normal PCT parameters; therefore,

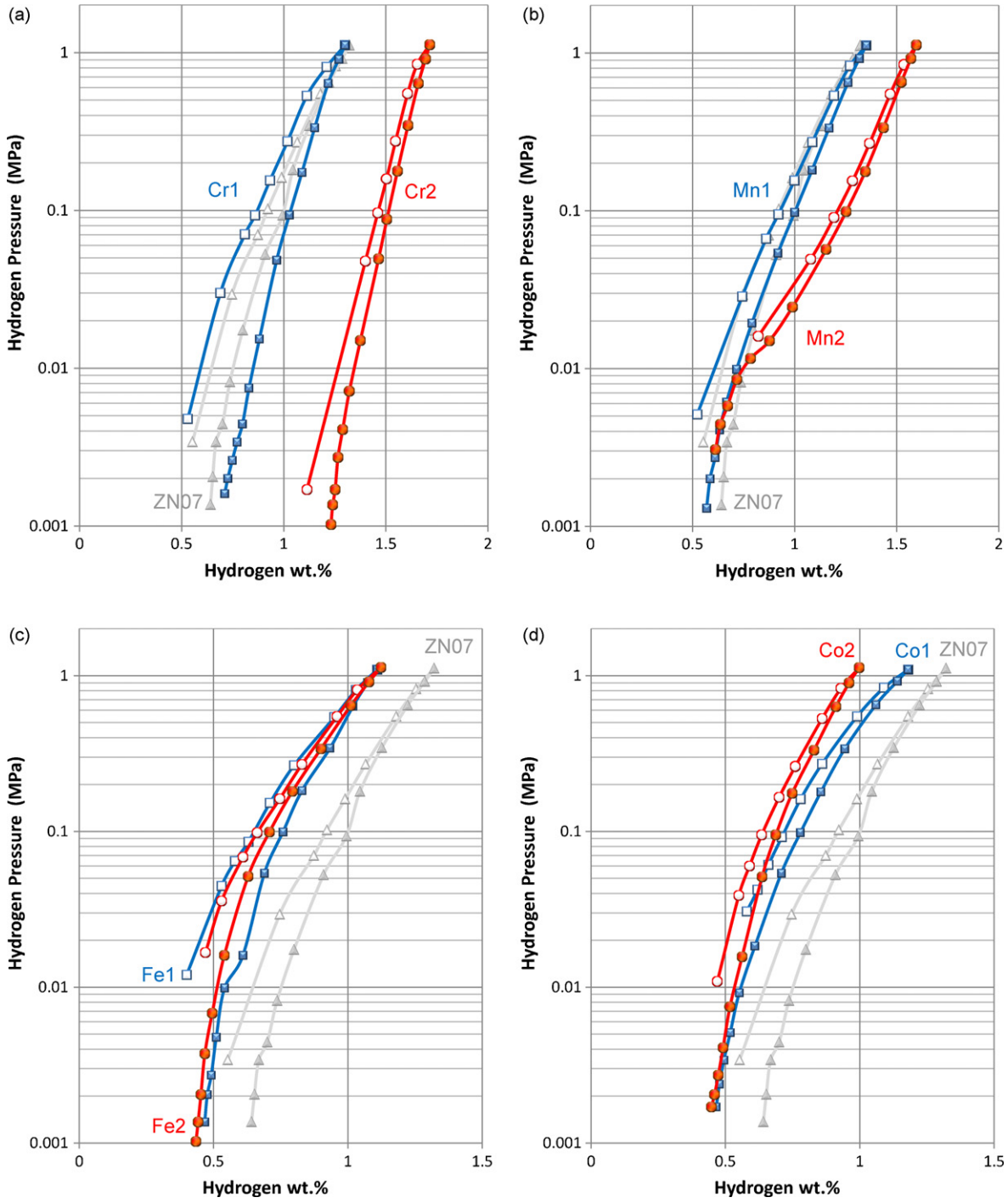

Fig. 1. 60 °C PCT isotherms of alloys Cr1 and Cr2 (a), Mn1 and Mn2 (b), Fe1 and Fe2 (c), Co1 and Co2 (d), Cu1 and Cu2 (e), Al1 and Al2 (f). Open and solid symbols are for absorption and desorption curves, respectively. Gray lines are isotherms from the base alloy, ZN07.

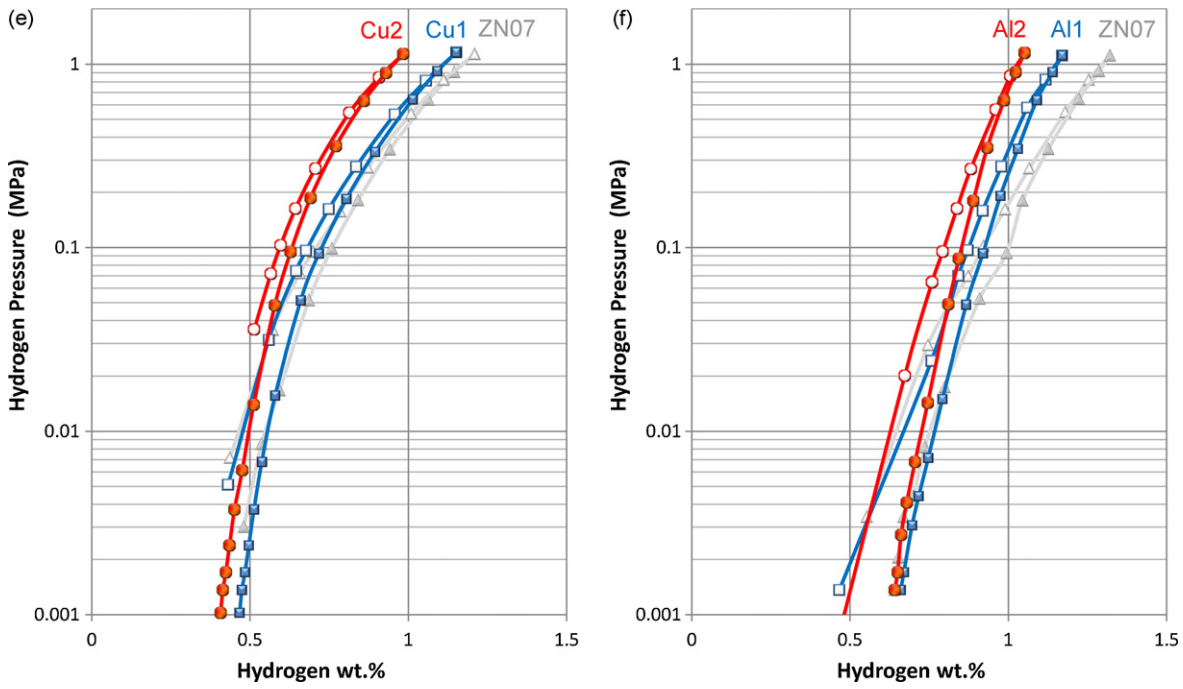

Fig. 1. (*Continued*)

PCT isotherms were measured at elevated temperature. All PCT-related properties of these alloys are listed in Table 1 and discussed below.

3.1.1. Hydrogen storage capacity

The maximum hydrogen storage capacity (up to a pressure of 1.2 MPa) at 60 °C for each of the alloys as a function of substitution level is shown in Fig. 3a. The maximum hydrogen storage does not change much at 10% substitution of Ni. At 20% substitution, Cr and Mn increase the maximum hydrogen storage while Al and Co decrease the maximum hydrogen storage. Cr and Mn are transition metals that have larger atomic radii and the larger size may help increase the hydrogen storage capability. Another possible explanation relates to the e/a value. Ivey and Northwood proposed that hydrogen storage capacity decreases with increasing e/a value [17]. Cr and Mn, modifiers with relatively small numbers of outer shell electrons, may contribute to the increase in storage capacity. Al, despite only having 3 valence electrons, has an equilibrium outer shell number of electrons of 10.4 when compared to the transition metals in the study of lattice constant ratio of a/c [18] and decreases the hydrogen storage capacity. From the CC listed in Table 2, ZrNi is the most beneficial phase for high maximum storage capacity. It also has the largest lattice expansion during hydriding [6]. Although the Zr_7Ni_{10} alloy absorbs more hydrogen than the Zr_9Ni_{11} alloy in the gas phase [19], there is no strong correlation between the abundances of Zr_7Ni_{10} and Zr_9Ni_{11} as constituent phases and the hydrogen storage capacity found in this study. From CC listed in Table 2, while C14 phase contributes positively to the maximum hydrogen storage capacity, the C15 phase has the opposite effect, which can be explained by the difference in e/a value. The C14 phase has a lower e/a value and as such has a higher storage capacity according to the argument given by Ivey and Northwood [17].

Reversible storage capacity is based on the desorption equilibrium pressure at 0.002 MPa. However, not all of the hydrogen can be desorbed completely at this pressure. The reversible hydrogen storage as a function of substitution amount is plotted in Fig. 3b. While most of the alloys show little or no improvement in reversible hydrogen storage, sample Mn2 exhibits an increase. According to the CC in Table 2, ZrNi phase is the only correlation that we can find to reversible storage capacity. Predictably, with the highest storage capacity, the storage in ZrNi becomes non-reversible. ZrNi was studied before and showed two very stable hydrides which required temperatures as high as 285 °C and 860 °C to dissociate [20–22]. The electrochemical discharge capacity of ZrNi alloy is only 30 mAh/g at a discharge current of 20 mA/g [19] and as such, the ZrNi phase is not desirable in an alloy requiring a high reversible storage capacity.

3.1.2. Mid-point pressure

The shapes of all the PCT isotherms in this study are very different from the conventional isotherm with a flat plateau region reported on most of simple hydrogen storage metals or alloys. As the number of elements in the alloy formula increases, the plateau region of the PCT isotherm becomes less distinctive, particularly compared to the plateau regions of binary alloys (Zr_7Ni_{10} from Ref. [4] and Zr_9Ni_{11} from Ref. [23]). Due to the lack of an identifiable flat region in the PCT isotherm, the mid-point pressure had been defined as the mid-point between the maximum storage capacity and the capacity at 0.002 MPa. Another alternative would be to take the pressure at a fixed concentration which was demonstrated previously to yield a similar result [24]. The mid-point pressure is related to the average hydrogen-metal bond strength and plotted against substitution level in Fig. 3c. Large modifiers, such as Mn and Al, make the hydride more stable and lower the mid-point pressure at higher substitution level. All the other modifiers make the hydride more unstable. In a design-matrix experiment with AB_2 alloys, Al was previously found to decrease the mid-point pressure while Co and Fe acted oppositely [24]. These previous findings are in total agreement with the results of this study. The CCs in Table 2 suggest that the C14 phase can effectively reduce the mid-point pressure while the C15 phase works oppositely. This result is in agreement with the conclusion from the study of quaternary alloys; C15 has weaker metal–hydrogen bond strength than C14

and improves the HRD of the alloy [5]. In general, C15 has a higher e/a value and is less likely to accept the extra electron donated from the hydrogen, therefore forming a less stable hydride.

3.1.3. Calculation of entropy and enthalpy

The mid-point pressure defined in the last section was used to estimate the heat of formation (ΔH) and the change in entropy (ΔS). We understand errors in calculation are very large and therefore the results are only good for a qualitative analysis. The calculation for sample Al1 and sample Al2 yield ΔS of −162 and −365 J/K mol H_2, respectively. Both values are too large for typical room temperature hydrogen storage materials [25] and were not included in Table 1. We believe the errors result from the wrong determination of plateau pressure. The remaining ΔH and ΔS values are listed in Table 1. Heat of formation (ΔH) is plotted against substitution level in Fig. 3d. Only Co and Fe substitutions increase the heat of formation and make the hydrides less stable, which is in agreement with the relatively lower total hydrogen storage capacity as shown in Fig. 3a. The larger substitutions of Cr and Mn decrease the heat of formation and make more stable hydrides, which is also in agreement with the increasing total hydrogen storage capacity as shown in Fig. 3a. The heats of

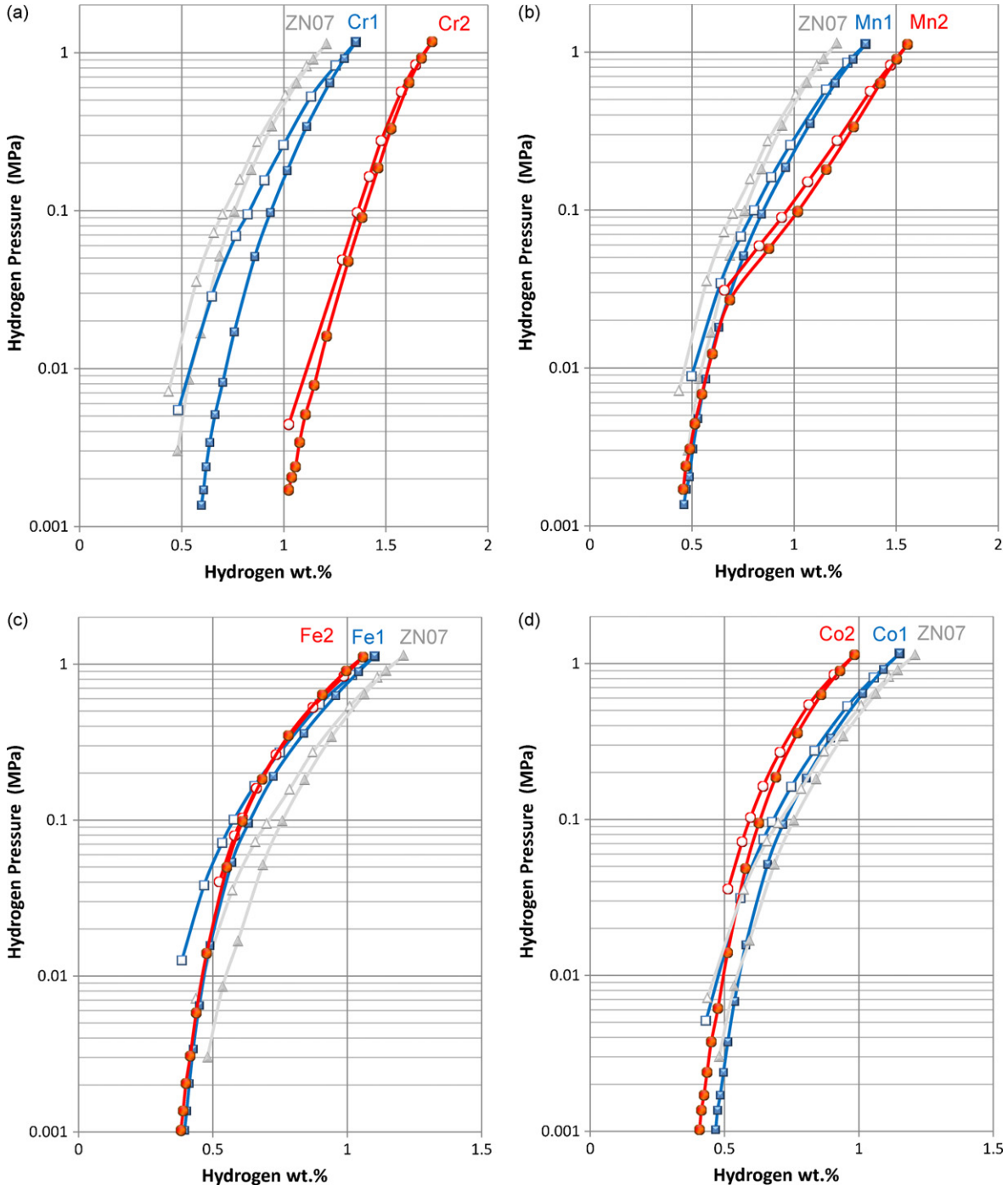

Fig. 2. 90 °C PCT isotherms of alloys Cr1 and Cr2 (a), Mn1 and Mn2 (b), Fe1 and Fe2 (c), Co1 and Co2 (d), Cu1 and Cu2 (e), Al1 and Al2 (f). Open and solid symbols are for absorption and desorption curves, respectively. Gray lines are isotherms from the base alloy, ZN07.

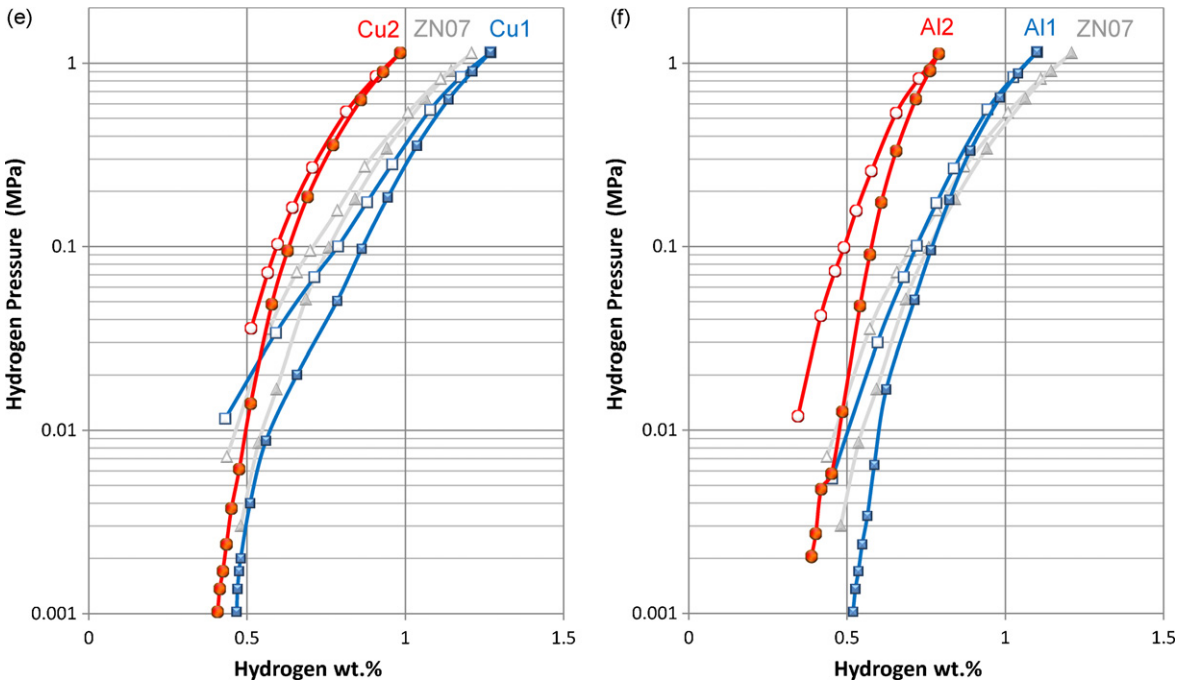

Fig. 2. (*Continued*)

formation of alloys with Cu and Al substitutions are very negative, and therefore the hydrides become highly irreversible (as indicated by XRD study after PCT analysis). The changes in the entropy for alloys with 10% substitution are similar to the base alloy, ZN07. As the substitution amount increases to 20%, all alloys, except for sample Co2 and sample Fe2, exhibit increase in the absolute value of entropy change, which indicates a more orderly hydride.

3.1.4. Slope factor

The slope of the PCT isotherm is related to the disordered nature of the material, which can be attributed to the number of phases [26], the complexity of the modifying elements [27], composition inhomogeneity [28–30], and domain sizes [31]. In this experiment, slope factor was calculated from the 60 °C desorption isotherm by taking the ratio of the capacities between the plateau region (defined between 0.005 and 0.2 MPa) and the entire reversible region. The measured slope factors are listed in Table 1 and also plotted against the substitution amount in Fig. 3e. Only Mn-substitutions show increase in the slope factor, and such results indicate more ordered structure and/or phase constitution. This special "homogenizing" power of Mn, as indicated by either a smoother PCT isotherm or a closer composition among constituent phases, has been seen not only in the AB_2 system [32,33], but also in the AB_5 [34], AB_3 [35], BCC [36], and Mg–Ni based AB alloys [37]. For the rest of the substitutions, the slope factor either stays about the same or decreases showing a higher degrees of disorder when more substitutional atoms are added into the alloy system. The reason for a large increase in slope factor between sample Cr1 and sample Cr2 may be due to the formation of the ZrNi phase with a chemical composition between two other major phases: Zr_9Ni_{11} and AB_2 (Table 4 in Ref. [6]). Since the disordered nature of the alloys depends more on the composition/structure variations among phases than on any individual phase, no correlation can be established between slope factor and the abundance of any particular phase. In other words, no phase contributes more to the homogeneity of the alloys than others.

3.2. Electrochemical properties

3.2.1. Half-cell capacity measurement

The discharge capacities for the 12 alloys in this study were measured. Capacities measured at the slowest discharge rate (4 mA/g) for the first 13 cycles for each alloy are plotted in Fig. 4a. Alloys with higher Mn and Co content activate faster than others due to the formation of oxides which are easily dissolved in the electrolyte, which is similar to the results for Mn and Co substitution in both AB_2 alloys [5] and AB_5 alloys [38]. The improvement in capacity by adding Mn into A_7B_{10} alloys has been demonstrated previously [39]. The capacity of most alloys shows improvement during the initial 13 formation cycles. Only sample Al2, with 20% substitution of Al, shows continuous capacity degradation due to the corrosive nature of the surface. Joubert et al. reported that in order to facilitate the activation process in a heterogeneous AB_2 alloy, the secondary phase (non-Laves phase in his case) must be homogeneously dispersed in the matrix (Laves phase) with a grain size less than 10 μm [40]. Despite the fact the matrix and secondary phase are just the opposite in the present study, it is expected that decreasing the grain size of the secondary phase will increase the grain boundary area and facilitate the activation process. However, when the micrographs from alloys with 10% and 20% substitution amounts are compared, sample Mn2, sample Fe2, sample Al2, and sample Al1 have larger secondary phase sizes but faster activations compared to the rest. Therefore, in the series of A_7B_{10} alloys in this study, the activation process is not governed by the grain size of the secondary phase.

The maximum capacity within the first 13 cycles for each alloy is listed in Table 1 and plotted against the substitution level in Fig. 5a. While both Mn and Fe contribute positively to the storage capacity, all other substitutions have a detrimental effect on the storage capacity. The best capacity of 349 mAh/g at a discharge current of 4 mA/g was obtained from alloy Mn2. This result is in agreement with the comparison of gas phase reversible hydrogen storage capacities. The electrochemical discharge capacity was converted to an equivalent hydrogen storage weight percent using the

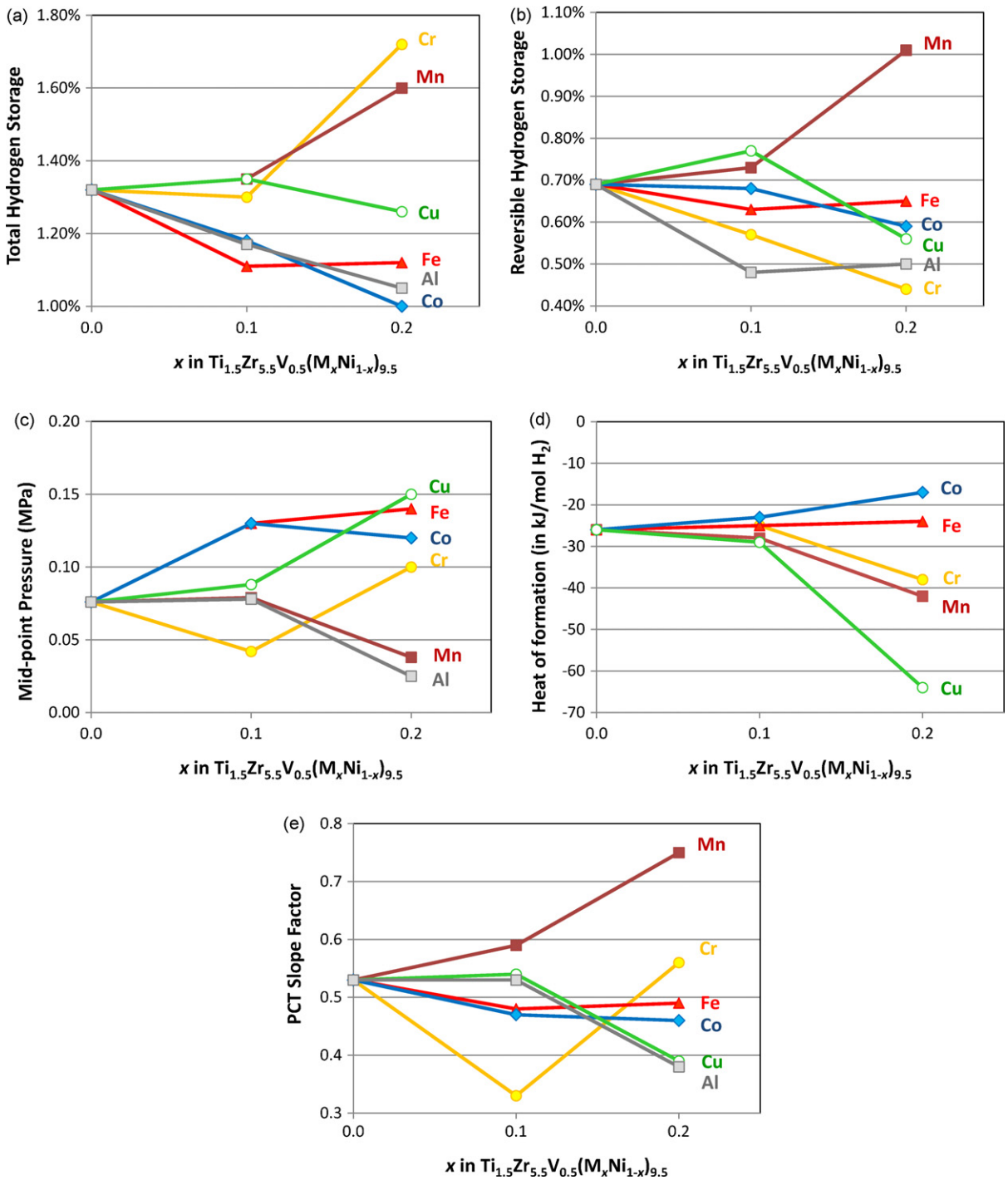

Fig. 3. The total hydrogen storage (a), reversible hydrogen storage (b), mid-point pressure (c), heat of formation (d), and PCT slope factor (e) as functions of substitution amount for all alloys in this study.

conversion factor:

$$1\ \text{wt.\% of}\ H_2 = 268\ \text{mAh/g} \quad (2)$$

The converted hydrogen storage weight percents are then plotted together with the maximum and reversible gas phase storage capacities in Fig. 6. Most of the electrochemical capacities lie between the maximum and reversible gas phase storage capacities. Both Fe-substituted alloys show closer values to the maximum gas phase capacities, which indicate better electrochemical catalytic effect from Fe. Sample Cu1 is the only alloy with an electrochemical discharge capacity lower than the reversible gas phase storage. The activation in sample Cu1 is particularly difficult, as observed from Fig. 4a. After 13 cycles, the capacity of sample Cu1 was still improving. The dips in sample Cu1 capacity in both Figs. 5a and 6 are due to slow activation. The difference in the surface evolution of sample Cu1 and sample Cu2 remains an interesting research topic and will be discussed in a separate paper. The correlation of discharge capacity to phase abundance is summarized in Table 2. Both C15 and Zr_9Ni_{11} phases have positive contributions to the discharge capacity while the Zr_7Ni_{10} phase has a negative contribution. This is in agreement with the comparison between the Zr_7Ni_{10} and Zr_9Ni_{11} alloys [19].

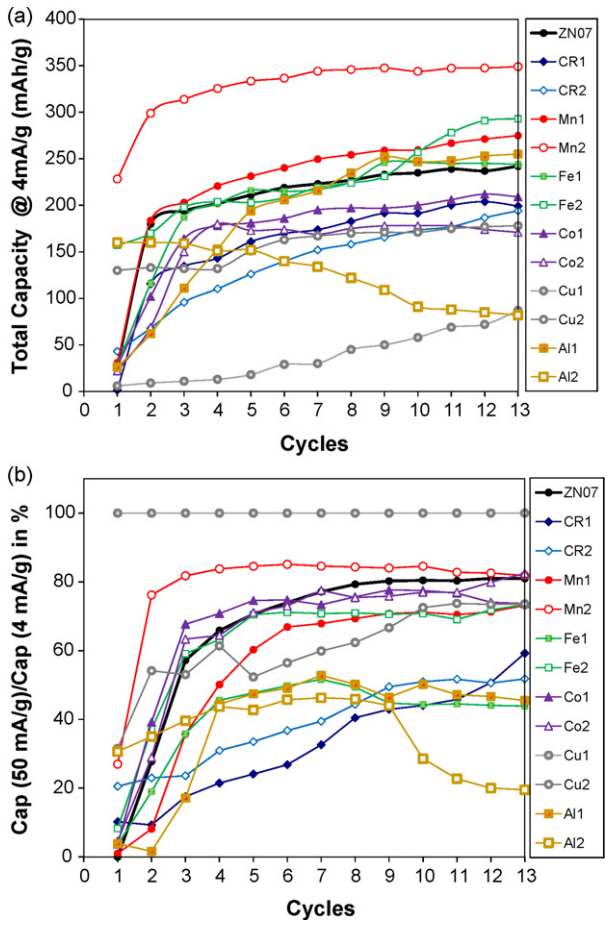

Fig. 4. Evolution of full discharge capacity at a rate of 4 mA/g (a) and ratio of capacities between 50 and 4 mA/g rates (b) as a function of cycle number for alloys in the study in comparison to the base alloy, ZN07.

HRD (the ratio between the capacities measured at high rate (50 mA/g) and low rate (4 mA/g)) is plotted in Fig. 4b for the first 13 cycles of each alloy. The general trend of the HRD evolution is similar to that of full capacity (Fig. 4a). As activation cycling continues, alloys break into smaller pieces; new surface is created and activated, improving both the capacity and speed of reaction. The HRD is plotted against the substitution level in Fig. 5b. Besides sample Cu1, which suffers from the lowest capacity, only sample Mn2 has a better HRD than that of the base ZN07. In the case of Cu1, the activation is very slow as can be seen from Fig. 4a. The as-prepared surface of Cu1 is electrochemically inactive. In this case, the creation of new surface dominates the evolution of capacity with cycling. All the electrochemical reaction happens on the newly developed surface from pulverization and therefore is very fast. With a limited active surface, the bulk transportation of hydrogen is not a limiting factor. In the mean time, the surface exchange current was measured when the alloy was fully activated. Therefore, the HRD of Cu1 is very high in the first 10 cycles in spite of its relatively inferior diffusion coefficient and surface exchange current.

Most of the modifiers do not improve the HRD, which suggests Ni is the most critical modifier determining the HRD. The correlation of HRD to phase abundance is summarized in Table 2. Of the non-Laves phases, Zr_7Ni_{10} is beneficial to high rate dischargeability but hinders discharge capacity due to its higher B-to-A ratio compared with Zr_9Ni_{11}. This result is different from the comparison of HRD in Zr_7Ni_{10} and Zr_9Ni_{11} alloys, which shows similar rate capabilities in a discharge current range from 25 to 320 mA/g [41]. When comparing the two Laves phases, C15 has better discharge capacity and rate capability. However, this conclusion should be limited to the A_7B_{10} stoichiometry because contradictory results were found for alloys with AB_2 stoichiometry [37].

3.2.2. Hydrogen diffusion coefficient measurement

Bulk hydrogen diffusion for various alloys was studied electrochemically using a previously reported potentiostatic discharge technique [4]. The diffusion coefficient (listed in Table 1) was calculated from the semi-logarithm of the current response vs. time in the later stage of measurement where the transport property was dominated by diffusion (time > 2000 s). The results are plotted against the substitution level in Fig. 5c. At 10% substitution, most of the alloys show a reduction in hydrogen diffusion coefficients (except for sample Mn1 and sample Al1). At 20% substitution, sample Mn2 shows the most improvement while sample Al2 shows the largest reduction. While sample Fe2 remains at the bottom of the comparison curve, sample Co2, sample Cr2 and sample Cu2 exhibit improvements in hydrogen diffusion. From previous studies on binary, ternary, and quaternary Zr_7Ni_{10} alloys, it was observed as the number of elements in the alloy increases, both the number of phases and the hydrogen diffusion coefficient increase [4,5]. For example, the hydrogen diffusion coefficient increases from 5.7×10^{-10} (Zr_7Ni_{10}), to 9.6×10^{-10} ($Ti_{1.5}Zr_{3.5}Ni_{10}$), and further to 18.9×10^{-10} cm^2/s ($Ti_{1.5}Zr_{3.5}V_{0.5}Ni_{9.5}$). However, hydrogen diffusion coefficients reach a saturated value after four elements. Except for sample Mn2, the additional modifier with a larger atomic radius used in quinary alloys does not significantly improve the hydrogen diffusion coefficient. At four elements, the density of transportation paths following the grain boundary may saturate the alloy. Comparison of SEM micrographs between two alloys with the same substituent element but different concentrations confirms this argument. Chen et al. reported the existence of the interface between Laves phase and non-Laves phase is important for hydrogen diffusion in the bulk [42]. However, there is no report directly linking the density of the grain boundary to the bulk transport property of hydrogen. There is no clear correlation between the grain size of the secondary phase and the bulk transport properties. Only the abundance of C14 phase shows some marginal correlation with the hydrogen diffusion coefficient. In previous studies in quaternary alloys, C14 phase was also found to contribute positively to hydrogen diffusion coefficient. Sample Mn2 has a large amount of C14 phase (50%) and therefore a large hydrogen diffusion coefficient. Sample Al2, although also dominated by C14 phase (70%), suffers from too strong metal–hydrogen bond strength and therefore has a very low hydrogen diffusion coefficient.

3.2.3. Exchange current measurement

The exchange current (I_0), a measure of the kinetics in the electrochemical hydrogen reaction at the surface of the electrode, was calculated from the polarization of electrodes by a previously published method [4]. The exchange currents measured at 50% state of charge for the alloys in this study are shown in Table 1. The results are plotted against substitution level in Fig. 5d. All quinary alloys in this study show smaller exchange currents than the base alloy ZN07. Ni-content is very critical to the surface reaction. In the previous study on quaternary alloys, a small amount of Ni replaced by V can improve the exchange current by a large amount due to the introduction of the C15 secondary phase [5]. Further replacement of Ni by V reduces the exchange current. The same trend extends to quinary alloys in this study. As the level of substitution increases from 10% to 20%, most alloys show improvement in the exchange current (except for sample Al2 and sample Cu2) due to the formation of less corrosion-resistant oxides in alkaline solution [43]. From Table 2, it can be seen that Zr_7Ni_{10} has a positive contribution

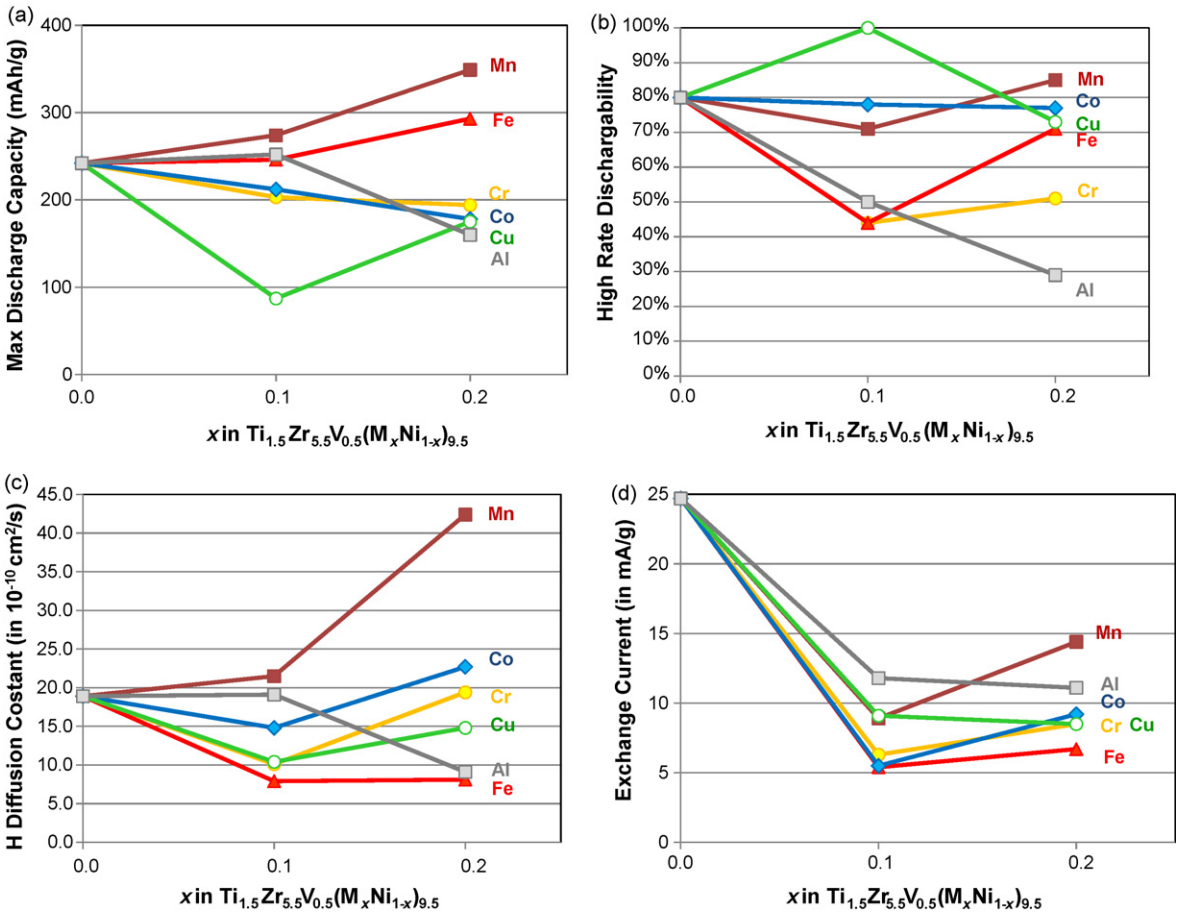

Fig. 5. The maximum discharge capacity (a), high rate dischargeability (b), hydrogen diffusion constant (c), and exchange current (d) as functions of substitution amount for all alloys in this study.

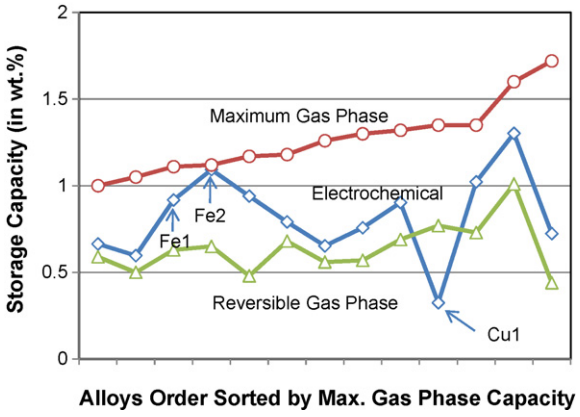

Fig. 6. Comparison among maximum gas phase storage capacity, reversible gas phase capacity, and electrochemical discharge capacity.

to the surface exchange current while Zr_9Ni_{11} has a negative contribution. Both of these two phases are low in vanadium and other substitutional elements. Their different Ni-contents contribute to the variation in the surface exchange currents. Also, C15 was found to be detrimental to the exchange current.

4. Summary

The effects of various modifier elements to the properties of a series of $(TiZr)_7(VNiX)_{10}$ alloys can be summarized in the following ordered lists according to their positive contributions:

In gas phase:

Maximum capacity: Cr > Mn > Ni > Cu > Fe ~ Al ~ Co
Reversible capacity: Mn > Ni > Fe ~ Co ~ Cu > Al ~ Cr
Mid-point pressure: Cu ~ Fe ~ Co > Ni ~ Cr (20%) > Cr (10%) ~ Mn ~ Al
Heat of formation: Co > Fe > Ni > Cr > Mn > Cu > Al (from unstable to stable)
Change in entropy: Co > Ni ~ Fe ~ Cr (10%) ~ Mn (10%) ~ Cu (10%) > Cr (20%) ~ Mn (20%) ~ Cu (20%) > Al (from less to more ordered)
Slope factor: Mn > Cr (20%) ~ Ni ~ Cu (10%) ~ Al (10%) > Fe ~ Co > Cu (20%) ~ Al (20%)

In electrochemical environment:

Activation: Mn > Co > Fe > Ni > Cr > Cu > Al
Total discharge capacity: Mn > Fe > Ni > Cu ~ Al ~ Cr ~ Co
High rate dischargeability: Mn ~ Ni ~ Co ~ Cu > Fe > Cr > Al
Hydrogen diffusion: Mn > Ni ~ Al (10%) > Co > Cr > Cu > Al (20%) > Fe
Exchange current: Ni > Mn > Al > Co ~ Cr ~ Cu ~ Fe

The contribution of various phases to the gas phase and electrochemical properties can be summarized by:

Zr_7Ni_{10}: Beneficial to both the high rate dischargeability and exchange current but detrimental to the discharge capacity, providing a more active surface.

Zr_9Ni_{11}: Just the opposite of Zr_7Ni_{10}, detrimental to both the high rate dischargeability and exchange current but beneficial to discharge capacity.

ZrNi: Only available from Cr2 (20%), beneficial to total gas phase storage capacity but detrimental to the hydride/dehydride reversibility.

C14: Beneficial to the gas phase storage and hydrogen diffusion, decreases heat of formation, entropy, mid-point pressure, and electrochemical high rate dischargeability; a more stable hydride.

C15: Beneficial to the electrochemical discharge capacity, detrimental to gas phase storage capacity and surface exchange current, increases heat of formation, entropy, and mid-point pressure.

References

[1] F.H.M. Spit, J.W. Drijver, W.C. Turkenburg, S. Radelaar, J. Phys. 41 (1980) C8–890.
[2] F.H.M. Spit, J.W. Drijver, S. Radelaar, Scr. Metall. 14 (1980) 1071.
[3] H. Sawa, K. Ohzeki, M. Ohta, H. Nakano, S. Wakao, Z. Phys. Chem. Neue Folge 164 (1989) 1527.
[4] K. Young, T. Ouchi, Y. Liu, B. Reichman, W. Mays, M.A. Fetcenko, J. Alloys Compd. 480 (2009) 521.
[5] K. Young, T. Ouchi, M.A. Fetcenko, W. Mays, B. Reichman, Int. J. Hydrogen Energy 34 (2009) 8695.
[6] K. Young, T. Ouchi, B. Huang, J. Nei, Y. Liu, M.A. Fetcenko, J. Alloys Compd. 501 (2010) 236.
[7] X.B. Zhang, D.Z. Sun, W.Y. Yin, Y.J. Chai, M.S. Zhao, Electrochim. Acta 50 (2005) 2911.
[8] S. Bliznakov, E. Lefterova, N. Dimitrov, Int. J. Hydrogen Energy 33 (2008) 5789.
[9] D.P. Smith, Hydrogen in Metals, The University of Chicago, Chicago, IL, USA, 1948.
[10] S.R. Ovshinsky, M.A. Fetcenko, J. Ross, Science 260 (1993) 176.
[11] M.A. Fetcenko, S.R. Ovshinsky, B.S. Chao, B. Reichman, US Patent 5,536,591 (1996).
[12] M.A. Fetcenko, S.R. Ovshinsky, K. Young, B. Reichman, C. Fierro, J. Koch, W. Mays, T. Ouchi, B. Sommers, A. Zallen, J. Alloys Compd. 330–332 (2002) 752.
[13] M.A. Fetcenko, S.R. Ovshinsky, K. Young, B. Reichman, T. Ouchi, J. Koch, W. Mays, US Patent 6,830,725 (2004).
[14] K. Young, M.A. Fetcenko, B. Huang, R.K. Regmi, G. Lawes, Y. Liu, J. Alloys Compd., submitted.
[15] K. Young, T. Ouchi, M.A. Fetcenko, J. Alloys Compd. 476 (2009) 774.
[16] K. Young, M.A. Fetcenko, F. Li, T. Ouchi, J. Alloys Compd. 464 (2008) 238.
[17] D. Ivey, D.O. Northwood, Mater. Lett. 2 (1983) 160.
[18] K. Young, T. Ouchi, M.A. Fetcenko, J. Alloys Compd. 480 (2009) 440.
[19] J.M. Joubert, M. Latroche, A. Percheron-Guégan, J. Bouet, J. Alloys Compd. 240 (1996) 219.
[20] G.G. Libowitz, H.F. Hayes, R. Gibbth Jr., J. Phys. Chem. 62 (1958) 76.
[21] S.L. Isaack, H.I. Shaaban, F.H. Hammad, Hydrogen Energy Progress V, in: T.N. Veziroglu, J.B. Taylor (Eds.), Proceeding of the 5th World Hydrogen Energy Conference, Toronto, Canada, July 15–20, 1984, International Association for Hydrogen Energy, 1984, p. 1443.
[22] S. Wakao, H. Sawa, H. Nakano, S. Chubachi, M. Abe, J. Less-Comm. Met. 131 (1987) 311.
[23] Z. Shi, M. Zeng, H. Kang, Atom. Energy Sci. Technol. 36 (2002) 439.
[24] K. Young, M.A. Fetcenko, J. Koch, K. Morii, T. Shimizu, J. Alloys Compd. 486 (2009) 559.
[25] L. Schlapbach, A. Züttle, Nature 414 (2001) 353.
[26] S. Lee, J. Yu, H. Lee, K. Jang, J. Lee, J. Alloys Compd. 293–295 (1999) 601.
[27] Z. Dehouche, M. Savard, F. Laurencelle, J. Goyette, J. Alloys Compd. 400 (2005) 276.
[28] K. Young, T. Ouchi, J. Koch, M.A. Fetcenko, J. Alloys Compd. 477 (2009) 749.
[29] C.N. Park, S. Luo, T.B. Flanagan, J. Alloys Compd. 384 (2004) 203.
[30] S. Luo, C.N. Park, T.B. Flanagan, J. Alloys Compd. 384 (2004) 208.
[31] K. Young, M.A. Fetcenko, F. Li, T. Ouchi, J. Koch, J. Alloys Compd. 468 (2009) 482.
[32] H.W. Yang, S.N. Jeng, Y.Y. Wang, C.C. Wan, J. Alloys Compd. 227 (1995) 69.
[33] Y.S. Hsu, S.L. Chiou, T.P. Perng, J. Alloys Compd. 313 (2000) 263.
[34] N. Mani, S. Ramaprabhu, J. Alloys Compd. 363 (2004) 275.
[35] B. Liao, Y.Q. Lei, L.X. Chen, G.L. Lu, H.G. Pan, Q.D. Wang, J. Alloys Compd. 376 (2004) 186.
[36] X.P. Song, P. Pei, P.L. Zhang, G.L. Chen, J. Alloys Compd. 455 (2008) 392.
[37] K. Young, unpublished.
[38] H. Teraoka, presented in Batteries, Nice, France, September 26–28, 2007. Article available from http://www.eneloop.info/fileadmin/EDITORS/ENELOOP/ARTICLES/Teraoka_Article_EN.pdf.
[39] I. Noriyasu, Japan Patent Hei6-57358 (1994).
[40] J.M. Joubert, D. Sun, M. Latroche, A. Percheron-Guégan, J. Alloys Compd. 253–254 (1997) 564.
[41] F.C. Ruiz, E.B. Castro, S.G. Real, H.A. Peretti, A. Visintin, W.E. Triaca, Int. J. Hydrogen Energy 33 (2008) 3576.
[42] L. Chen, F. Wu, M. Tong, D.M. Chen, R.B. Long, Z.Q. Shang, H. Liu, W.S. Sun, K. Yang, L.B. Wang, Y.Y. Li, J. Alloys Compd. 293–295 (1999) 508.
[43] M. Pourbaix, Atlas of Electrochemical Equilibria in Aqueous Solution", 2nd English edition, NACE, Houston, TX, USA, 1974.